IEEE Access
Multidisciplinary | Rapid Review | Open Access Journal

Received June 26, 2019, accepted July 19, 2019, date of publication July 30, 2019, date of current version August 14, 2019.

*Digital Object Identifier 10.1109/ACCESS.2019.2932021*

# Influence of Surface Roughness on the Pump Performance Based on Computational Fluid Dynamics

**XIAOKE HE[1], WEIXUAN JIAO[2], CHUAN WANG[1,2], AND WEIDONG CAO[3]**

[1]School of Electric Power, North China University of Water Resources and Electric Power, Zhengzhou 450045, China
[2]College of Hydraulic Science and Engineering, Yangzhou University, Yangzhou 225002, China
[3]Institute of Fluid Engineering Equipment, JITRI, Jiangsu University, Zhenjiang 212013, China

Corresponding author: Chuan Wang (wangchuan198710@126.com)

This work was supported in part by the National Natural Science Foundation of China under Grant 51609105, in part by the Project of Key Research and Development in Zhenjiang under Grant SH2017049, in part by the Henan Province Education "The 13th Five-Year Plan" Project of Year 2016 under Grant 2016-JKGHA-0017, in part by the Open Fund of Key Laboratory of Water-Saving Agriculture of Henan Province under Grant FIRI2016-19-01, and in part by the Priority Academic Program Development of Jiangsu Higher Education Institutions (PAPD).

**ABSTRACT** The influence of surface roughness on the pump performance was deeply analyzed based on computational fluid dynamics (CFD). A series of numerical calculations with different grid numbers, turbulence models, and surface roughness were made for a typical multistage centrifugal pump. Moreover, the external characteristic experiments were also conducted to verify the numerical calculations. The results show that the surface roughness has enormous influences on the pump performance. With the increase of the surface roughness, the head and the efficiency of the pump decreases continuously, but the decreasing rate slows down gradually, and the surface roughness has a greater influence on the efficiency than that on the head. Moreover, the influence of surface roughness on the disk friction loss power is much greater than that on the hydraulic power. Besides, the total efficiency of the pump reduces mainly by decreasing the hydraulic efficiency and the mechanical efficiency, due to the negative effect of surface roughness. In addition, the surface roughness of the impeller and the diffuser mainly affects the hydraulic efficiency, the surface roughness of the shroud's outer wall mainly influences the mechanical efficiency, and the surface roughness of the inner wall of the pump cavity mainly affects the volume efficiency, but the influence of surface roughness on the pump performance is interconnected. Therefore, due to that, it's very difficult to make the precision-machine inside the impeller and diffuser, polishing the impeller shroud and pump cavity is beneficial to improve the pump efficiency and reduce the pump shaft power.

**INDEX TERMS** Mechanical engineering, pump, surface roughness.

## I. INTRODUCTION

Pumps are classified as general machinery with varied applications. According to statistics, the energy consumption of pumps accounts for nearly 22% of the world's energy used by electric motors; thus, pumps have huge energy consumption and considerable energy-saving potential [1]–[7]. In the past several years, an increasing number of energy-saving strategies have been proposed, and end-users have pushed industries and researchers to concentrate on improving the pump efficiency to save energy [8]–[14]. Moreover, multistage centrifugal pumps have attracted increasing attention as fundamental elements for providing high-energy liquid recently, which have been used in rural area, field irrigation, geothermal utilization and so on [15]–[24].

In the early research, developing excellent hydraulic model was the most common way to improve the pump efficiency. However, when the pump efficiency reaches a relatively high condition, it becomes much difficult to do the further optimization work. As with the flow in a pipe, energy loss in the pump depends on Reynolds number and relative surface roughness, so the pump efficiency is obviously affected by some parameters such as pump size, fluid speed, fluid viscosity and surface roughness. Due to that the former

The associate editor coordinating the review of this manuscript and approving it for publication was Zhixiong Peter Li.

  

third parameters depend on the end-users' requirement, it's rather difficult to make great change for them. As a result, the surface roughness plays a more and more important role in improving the pump efficiency. Stepanov [25] mentioned that, for small centrifugal pumps, the efficiency could be improved by 2% to 4% if the volute channel was cleaned up. Lomakin [26] provided an example of a large casting pump, of which the efficiency increased from 78% to 89% after polishing its flow parts. Li and Wang [27] made the numerical investigation about the effect of surface roughness on one axial pump, and found that the pump efficiency decreased from 84% to 70% when the surface roughness increased from 0 to 0.6 mm, reflecting that the surface roughness had a great influence on the pump efficiency. However, most previous studies only concentrated on the simple influence of surface roughness on the pump's overall performance by doing experiments or numerical calculations, and lacked of detailed analysis how the surface roughness influenced the pump performance. Therefore, it's necessary to make in-depth study, overlaying multiple perspectives, on the relationships between the surface roughness and the pump performance, which is the aim of the present study.

At present, Computational Fluid Dynamics (CFD) is frequently used in the simulation of the flow field [28]–[30]. CFD optimization guides the pump optimization by simulating the three-dimensional incompressible flow field of the pump using a high-performance computer [31], [32]. In recent years, researchers have made the preliminary design and subsequently applied CFD optimization. Wang *et al.* [33] combined a 3D inverse design method, CFD calculations and multi-objective optimization strategy to construct an optimal design system for improving the performances of a reversible pump-turbine runner. Anagnostopoulos [34] developed a numerical optimization algorithm based on the unconstrained gradient approach and combined with the evaluation software in order to find the impeller geometry that maximizes the pump efficiency. The results verified that the optimization process can converge very fast and to reasonable optimal values. Kim *et al.* [35] obtained an optimized impeller which satisfied the design specifications according to a response surface method (RSM) analysis, and the performance of the optimized impeller was verified through numerical analysis. Derakhshan *et al.* [36] developed an efficient and original approach to improve the performance of a Berkeh 32-160 pump based on the Artificial Neural Networks (ANNs) and Artificial Bee Colony (ABC) algorithm. As reviewed above, CFD optimization is not restricted by physical model and test apparatus, which saves time and money substantially. Moreover, most of current numerical calculations can only predict the pump's overall performance, and fall short in detailed analysis of the various kinds of energy losses in the pump.

Therefore, in this paper the influence of surface roughness on the pump performance was analyzed by varying working condition, rotational speed and effecting location of surface roughness. This paper provides a new way to improve the performance of multistage centrifugal pump.

## II. SETTING METHODS FOR NUMERICAL CALCULATION

CFD is suitable for simulating the internal flow field of rotating machinery. Nevertheless, the numerical settings of CFD should be selected appropriately to ensure the reliability of results. Therefore, a series of numerical calculations for a typical multistage centrifugal pump were performed using different grid numbers and turbulence models.

### A. HYDRAULIC DESIGN OF THE IMPELLER AND DIFFUSER

Impellers and diffusers are the core components of centrifugal pumps. The geometric parameters of impellers and diffusers can be obtained using velocity coefficient method, as shown in Table 1. The inlet angle of positive diffuser blades has a small value of $\alpha_3 = 5°$ to extend the flow channel of the positive diffuser. Reducing the outlet angle of the return diffuser blade will help obtain a steeper head-flow rate curve, lower maximum shaft power [37]. Thus, the outlet angle of the return diffuser blades was set to 50°. Table 1 shows that the two-dimensional models of the impeller and diffuser can be obtained, as respectively shown in Figures 1 and 2.

**TABLE 1. Basic geometric parameters of the pump.**

| Geometric parameter | Value | Geometric parameter | Value |
|---|---|---|---|
| Inlet diameter of the impeller $D_1$ (mm) | 20 | Outlet width of the impeller blade $b_2$ (mm) | 3 |
| Hub diameter of the impeller $D_{hb}$ (mm) | 33.5 | Number of outward diffuser blades $Z_p$ | 9 |
| Outlet diameter of the impeller $D_2$ (mm) | 108 | Number of return diffuser blades $Z_n$ | 9 |
| Inlet angle of the impeller blade $\beta_1$ (°) | 40 | Inlet diameter of the outward diffuser $D_3$ (mm) | 109 |
| Outlet angle of the impeller blade $\beta_2$ (°) | 15 | Inlet angle of the outward diffuser blade $\alpha_3$ (°) | 5 |
| Wrap angle of the impeller blade $\theta_w$ (°) | 150 | Outlet angle of the return diffuser blade $\alpha_6$ (°) | 50 |
| Number of the impeller blades $Z$ | 8 | Rated flow $Q_r$ ($m^3$/h) | 3.3 |
| Rotational speed of the impeller $n$ (r/min) | 2800 | Stage number of the multistage pump | 5 |

### B. ESTABLISHING THE CALCULATION DOMAIN

The stage number of multistage centrifugal pumps depends on user demands. If the flow field of the calculation model with all the stage is simulated, the grid number becomes too large to meet the requirements of a practical engineering application. In addition, multistage centrifugal pumps are more complicated than single-stage centrifugal pumps. The swirling of the inlet flow of the impellers, except for the first one, is caused by the outlet flow of diffusers. The two-stage pump was selected in this study considering the increase of grid number with the increase of the pump stage.

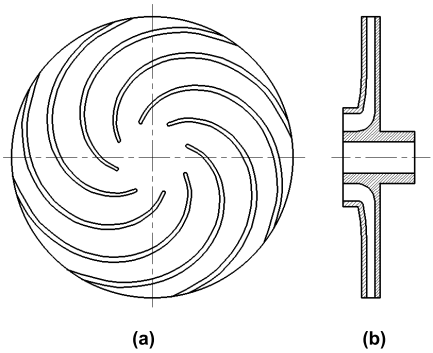


**FIGURE 1.** Two-dimensional diagram of the impeller: (a) plane projection; (b) axial projection.

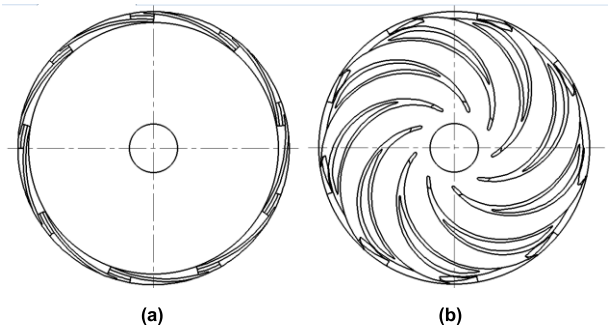


**FIGURE 2.** Two-dimensional diagram of the diffuser: (a)outward diffuser; (b) return diffuser.

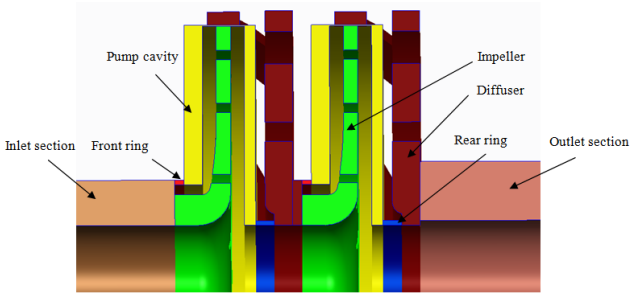


**FIGURE 3.** Calculation domain of the two-stage pump.

Figure 3 shows that the calculation domain of the two-stage pump includes the inlet section, two impellers, two pump cavities, two diffusers, two front rings, two rear rings, and the outlet section. The lengths of the inlet and outlet sections are respectively five and four times of the diameter of the impeller.

This analysis suggests that the predicted external characteristics of the multistage pump depend on the parameters of the two-stage pump, which are shown as follows:

$$H = H_{\text{in}} + H_1 + (N-1)H_2 + H_{\text{out}} \quad (1)$$

$$P = P_1 + (N-1)P_2 \quad (2)$$

$$\eta = \frac{\rho g Q H}{P} \quad (3)$$

where $H$ is the total head of the multistage pump (in m); $H_{\text{in}}$ is the loss head of the inlet section (in m); $H_1$ is the head of the first stage (in m); $H_2$ is the head of the second stage (in m); $H_{\text{out}}$ is the loss head of the outlet section (in m); $Q$ is the flow rate (in $m^3/h$); $P$, $P_1$, and $P_2$ are the shaft power values of the multistage pump, and the first and second stages (in W), respectively; and $\eta$ is the efficiency of the multistage pump. The calculation results are then translated (through an appropriate procedure) to extrapolate the five-stage pump, for which the experimental data are available and discussed hereinafter.

### C. ANALYZING GRID INDEPENDENCE

The calculation domain should be discretized before simulation based on grids. In this study, the calculation domain was divided into structured grids by ICEM CFD software. Theoretically, the calculating errors would decrease gradually with an increase in grid number; however, too many grids would pose prohibitive demands on computational resources and time. Five grid sizes ($G$) with the same numerical settings (surface roughness $\mu = 1$ $\mu$m) were selected to determine the appropriate grid number. The results under rated flow conditions of $Q = 3.3$ $m^3/h$ are shown in Table 2. Due to that the pump generally works under nearly rated flow condition, so small flow condition and large flow condition are not included herein.

**TABLE 2.** Grid independence test of the pump under rated flow condition.

| Grid size $G$ (mm) | 1.5 | 1.2 | 1.0 | 0.8 | 0.7 |
|---|---|---|---|---|---|
| Grid number | 1321154 | 1773142 | 2399892 | 3674514 | 4839030 |
| Node number | 1146888 | 1537022 | 2091526 | 3233200 | 4289372 |
| $\eta$ (%) | 42.19 | 41.79 | 41.43 | 41.13 | 41.15 |
| $H$ (m) | 42.11 | 41.99 | 41.62 | 41.62 | 41.64 |

It can be seen that the grid size minimally influences the numerical results, and the overall difference is within 2%. The efficiency $\eta$ and total head $H$ are slightly high when the grid size is relatively large ($G \geq 1.0$ mm) and are basically stable when $G \leq 0.8$ mm. G is set to 0.8 mm after considering the computational accuracy and time, and the structured grids of the calculation domain are shown in Figure 4. Of course, 0.8 mm grid size is not a universal principle that can be applied to all scenarios, because the grid size completely depends on the size of the calculation model and the requirement of the grid quality. In principle, grid independence should be made to obtain a suitable gird size for any new calculation models.

### D. SELECTING THE TURBULENCE MODEL

A universal turbulence model that is applicable for all flow problems has not yet been formulated; thus, scholars have selected different turbulence models for different turbulent

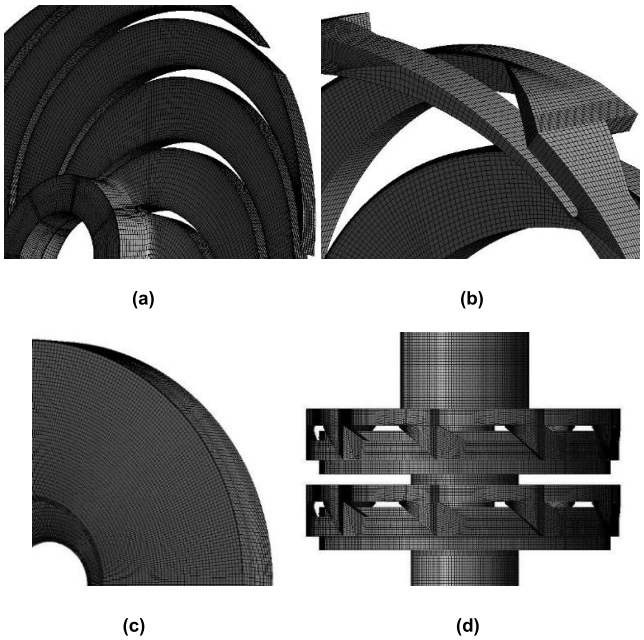


**FIGURE 4.** Structured grids of the calculation domain: (a) impeller; (b) diffuser; (c) pump cavity; (d) entire calculation domain.

flows. In this study, numerical calculations were performed with ANSYS CFX software, which provides a number of turbulence models. Among the turbulence models, $k$-$\varepsilon$ and $k$-$\omega$ are known to be the most suitable for the internal flow of rotating machines. Therefore, five models, i.e., standard $k$-$\varepsilon$, RNG $k$-$\varepsilon$, BSL $k$-$\omega$, standard $k$-$\omega$, and SST $k$-$\omega$, were selected, and their results were compared with the experimental results with the same numerical settings (surface roughness $\mu = 1$ $\mu$m). Table 3 shows the numerical and experimental results of the pump with different turbulent models under rated flow conditions of $Q = 3.3$ m$^3$/h. It can be found that, after comprehensive comparison, the prediction by standard $k$-$\varepsilon$ model is closest to the experimental data; thus, this model was selected in this study.

**TABLE 3.** Numerical and experimental results with different turbulent models under rated flow condition.

| Turbulence model | Standard $k$-$\varepsilon$ | RNG $k$-$\varepsilon$ | BSL $k$-$\omega$ | Standard $k$-$\omega$ | SST $k$-$\omega$ | Test value |
|---|---|---|---|---|---|---|
| $\eta$ (%) | 41.13 | 41.28 | 44.96 | 44.55 | 44.59 | 40.73 |
| $H$ (m) | 41.62 | 41.12 | 43.54 | 43.46 | 43.50 | 41.87 |

### E. SETTING OF BOUNDARY CONDITIONS

The impeller and the shroud in the pump cavity were based on the rotating reference frame, whereas the other sub-domains were based on the stationary reference frame throughout the entire calculation domains. The interfaces between the impeller and its adjacent sub-domains were set to ''Frozen Rotor'' mode, and the other interfaces were set to ''General Connection'' mode. Moreover, the non-slip walls were selected as the wall boundaries. The open inlet and mass outflow were selected as the inlet and outlet boundaries.

## III. INFLUENCE OF SURFACE ROUGHNESS ON THE PUMP PERFORMANCE

### A. EFFECT OF THE SURFACE ROUGHNESS ON THE HEAD AND EFFICIENCY OF THE PUMP

To study the effect of the surface roughness on the pump performance, different values of the surface roughness ($\mu = 0$, 1, 10, 20, 40 and 80 $\mu$m) were selected for the numerical calculation of the five-stage pump. The results were presented in Table 4. As can be seen, with the increase of $\mu$, $H$ and $\eta$ continue to decrease, but the decreasing rate of $\eta$ is significantly greater than that of $H$, indicating that the pump shaft power is also increasing. In addition, when $\mu$ is small, the decreasing rate of $\eta$ and $H$ reduces significantly, but slows down when $\mu$ is large. When $\mu$ increases from 0 $\mu$m to 80 $\mu$m, $\eta$ decreases from 41.67% to 28.96%, and $H$ decreases from 41.83 m to 35.91 m, with their amplitude decreased by 31.06% and 14.19% respectively. This demonstrates the significant influence of surface roughness on the numerical results. Therefore, in CFD suitable surface roughness should be selected according to the material properties, otherwise significant difference may appear. In this study, the pump was made of PPO (polyphenol oxidase) and stainless steel, where the value of $\mu$ is usually within 1 $\mu$m. Therefore, in the present study 1 $\mu$m is finally selected as the value of the surface roughness.

**TABLE 4.** Efficiency and head of the pump with different surface roughness at rated flow.

| Roughness $\mu$ (μm) | 0 | 1 | 10 | 20 | 40 | 80 | Test value |
|---|---|---|---|---|---|---|---|
| $\eta$ (%) | 41.67 | 41.13 | 37.71 | 35.34 | 32.46 | 28.96 | 40.73 |
| $H$ (m) | 41.83 | 41.62 | 40.27 | 39.25 | 37.83 | 35.91 | 41.87 |

### B. EFFECT OF THE SURFACE ROUGHNESS ON THE COMPONENT EFFICIENCY AND COMPONENT POWER OF THE PUMP

In order to study the reason why the surface roughness has such a great influence on the pump performance, the external characteristic parameters of the multistage pump was further subdivided. The efficiency of the pump should be divided into three kinds of component efficiencies, while the power of the pump should be divided into two kinds of component power. Ignoring the mechanical friction loss, the detailed parameters of each component efficiency and component power are shown in Table 5, and the formulas of component efficiency and component power are shown as follows.

$$P = P_{\mathrm{m}} + P_{\mathrm{h}} \tag{4}$$

$$P_{\mathrm{m}} = P_{1\mathrm{m}} + (N-1)P_{2\mathrm{m}} \tag{5}$$

$$P_{\mathrm{h}} = P_{1\mathrm{h}} + (N-1)P_{2\mathrm{h}} \tag{6}$$

**TABLE 5. Pump's component efficiency and component power with different roughness at rated flow.**

| $\mu$ (μm) | $P_m$ (W) | $P_h$ (W) | $P$ (W) | $q$ ($m^3$/h) | $\eta_m$ (%) | $\eta_v$ (%) | $\eta_h$ (%) |
|---|---|---|---|---|---|---|---|
| 0 | 184.16 | 717.66 | 901.82 | 0.68 | 79.58 | 82.98 | 63.10 |
| 1 | 189.55 | 719.57 | 909.12 | 0.69 | 79.15 | 82.78 | 62.77 |
| 10 | 226.39 | 732.91 | 959.30 | 0.75 | 76.40 | 81.50 | 60.56 |
| 20 | 255.43 | 742.11 | 997.54 | 0.78 | 74.39 | 80.85 | 58.76 |
| 40 | 291.93 | 755.01 | 1046.94 | 0.83 | 72.12 | 79.95 | 56.30 |
| 80 | 341.49 | 772.24 | 1113.74 | 0.88 | 69.34 | 79.03 | 52.86 |

$$q = \frac{q_1 + (N-1)q_2}{N} \tag{7}$$

$$\eta_m = 1 - \frac{P_m}{P} \tag{8}$$

$$\eta_v = \frac{Q}{Q+q} \tag{9}$$

$$\eta_h = \frac{\eta}{\eta_m \eta_v} \tag{10}$$

where $P$ is the shaft power of the multistage pump (in W), $P_m$ is the disk friction loss power of the multistage pump (in W), $P_h$ is the hydraulic power of the multistage pump (in W), $P_{1m}$ is the disk friction loss of the first-stage pump (in W), $P_{2m}$ is the disk friction loss of the second-stage pump (in W), $P_{1h}$ is the hydraulic power of the second-stage pump (in W), $P_{2h}$ is the hydraulic power for of the second-stage pump (in W), $q$ is the average ring leakage of the multistage pump (in $m^3$/h), $q_1$ is the ring leakage of the first-stage pump (in $m^3$/h), $q_2$ is the ring leakage amount of the second-stage pump (in $m^3$/h), $\eta_m$ is the mechanical efficiency, $\eta_v$ is the volumetric efficiency, and $\eta_h$ is the hydraulic efficiency.

Figure 5 shows the disk friction loss power $P_m$, the hydraulic power $P_h$ and the shaft power $P$ of the pump at rated flow condition with different surface roughness. Combined with Table 5, it can be found that, with the increase of $\mu$, three kinds of power increase together, but the increasing rate decreases gradually. If $\mu$ increases from 0 $\mu$m to 80 $\mu$m, $P_m$ increases from 184.16 W to 341.49 W, and $P_h$ increases from 717.66 W to 772.24 W. The increasing amplitudes of two kinds of component power are 85.44% and 7.61% respectively, which indicates that the influence of the surface roughness on the disk friction loss power is much greater than that on the hydraulic power.

Figure 6 shows the mechanical efficiency $\eta_m$, the hydraulic efficiency $\eta_v$ and the volume efficiency $\eta_h$ of the pump at rated flow condition with different surface roughness. Combined with Table 5, $\eta_v$ is the largest and $\eta_h$ is the smallest among three kinds of component efficiencies. With the increase of $\mu$, three kinds of component efficiencies decrease together, and the decreasing rate reduces constantly. When $\mu$ increases from 0 $\mu$m to 80 $\mu$m, $\eta_m$ decreases from 79.58% to 69.34%, $\eta_h$ decreases from 63.10% to 52.86%, and $\eta_v$ decreases from 82.98% to 79.03%. The decreasing amplitudes of three kinds of component efficiencies are 12.87%, 16.22% and 4.76 respectively, indicating that the total efficiency of the pump reduces mainly by decreasing the hydraulic efficiency and the mechanical efficiency, due to the negative effect of the surface roughness.

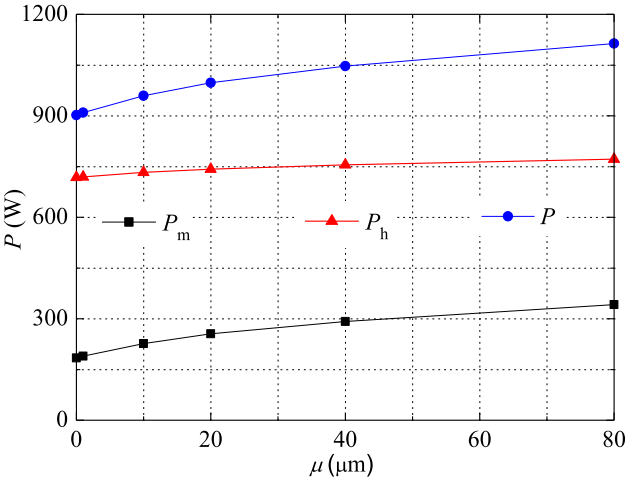


**FIGURE 5. Pump's disk friction loss, hydraulic and shaft power with different surface roughness.**

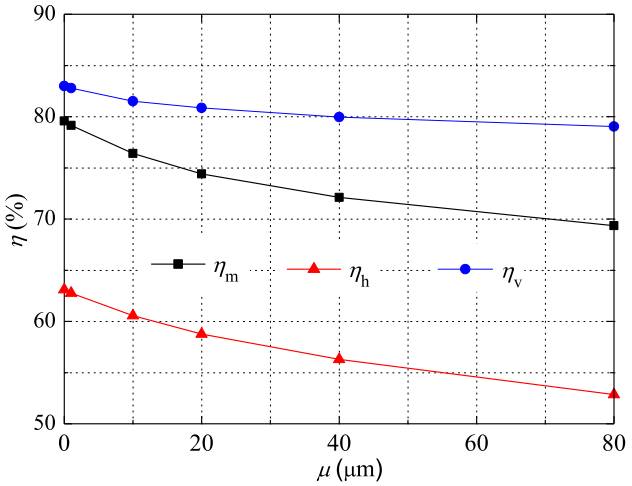


**FIGURE 6. Pump's mechanical, hydraulic and volume efficiency with different surface roughness.**

### C. THE INFLUENCE OF THE SURFACE ROUGHNESS OF THE FLOW PARTS ON THE PUMP PERFORMANCE

In order to study the influence of the surface roughness of the flow parts on the pump performance, the surface roughness were considered on the wall of four main flow parts, namely, impeller (including blade wall and inner wall), diffuser (including blade wall and inner wall), shroud and pump cavity. Different combination cases were calculated, and the value of the surface roughness was 40 $\mu$m. In case 1,

**TABLE 6. Pump's performance for different roughness groups at rated flow.**

| Rough flow parts | Case | $H$ (m) | $P_m$ (m) | $P_h$ (m) | $q$ ($m^3$/h) | $\eta_m$ (%) | $\eta_v$ (%) | $\eta_h$ (%) | $\eta$ (%) |
|---|---|---|---|---|---|---|---|---|---|
| No part | 1 | 41.83 | 184.16 | 717.66 | 0.68 | 79.58 | 82.98 | 63.1 | 41.67 |
| Impeller | 2 | 40.86 | 185.59 | 735.98 | 0.64 | 79.86 | 83.72 | 59.57 | 39.83 |
| Diffuser | 3 | 40.02 | 181.94 | 724.43 | 0.71 | 79.92 | 82.29 | 60.33 | 39.68 |
| Shroud | 4 | 39.27 | 275.2 | 714.86 | 0.59 | 72.2 | 82.98 | 64.02 | 39.27 |
| Cavity | 5 | 39.32 | 195.05 | 729.61 | 0.94 | 78.91 | 77.76 | 62.27 | 38.2 |
| Shroud and cavity | 6 | 40.13 | 294.31 | 727.86 | 0.85 | 71.21 | 79.56 | 63.22 | 35.84 |
| All parts | 7 | 37.83 | 291.93 | 755.01 | 0.83 | 72.12 | 79.95 | 56.3 | 32.46 |

the surface roughness for all the flow parts was neglected. In case 7, the surface roughness for all the flow parts was considered. In other cases, the surface roughness for some flow parts was considered. The numerical results are shown in Table 6.

Figure 7 shows the head $H$ and the efficiency $\eta$ of the pump for different roughness groups at rated flow condition. Combined with Table 6, it can be found that $\mu$ will make $H$ and $\eta$ reduce together. The influence order of $\mu$ on $H$ is impeller, diffuser, shroud and pump cavity in sequence, while that on $\eta$ is successively impeller, diffuser, pump cavity and shroud. However, if the shroud and the pump cavity are both set as rough (In case 6), the comprehensive influence of $\mu$ on $H$ is smaller than that of the single flow part (In case 4 or case 5). It indicates that the influence of the surface roughness of the flow parts on the pump performance is not independent, but interconnected.

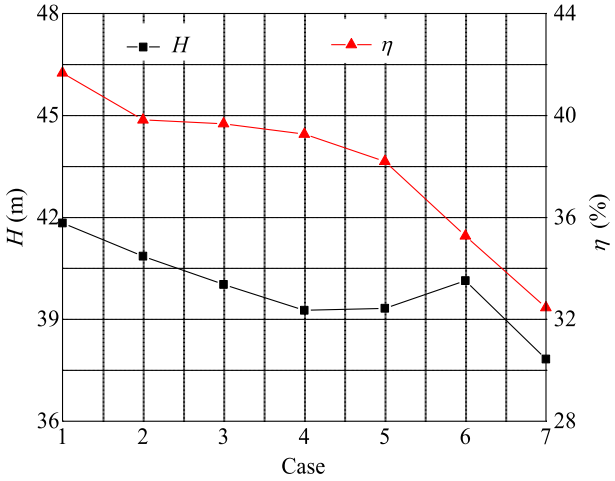


**FIGURE 7. Pump's head and efficiency for different roughness groups.**

Figure 8 shows the disk friction loss power $P_m$, the hydraulic power $P_h$ and the shaft power $P$ of the pump for different roughness groups at rated flow condition. Combined with Table 6, it can be found that $\mu$ will make $P_m$ and $P$ increase obviously, while $P_h$ almost keeps stable. The surface roughness of the outer wall of the shroud has

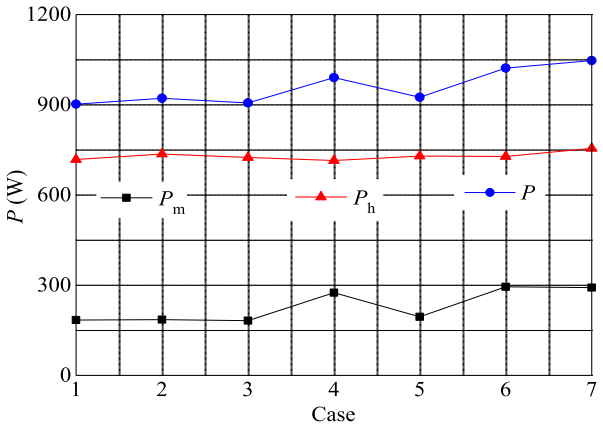


**FIGURE 8. Pump's disk friction loss, hydraulic and shaft power for different roughness groups.**

the most significant effect on $P_m$ (Seen in case 4). When case is changed from 1 to 4, $P_m$ increases from 184.16 W to 275.20 W. When case is changed from 1 to 7, $P_m$ increases from 184.16 W to 291.93 W, and $P$ increases from 901.82 W to 1046.94 W. Therefore, the disk friction loss caused by the surface roughness of the shroud accounts 84.48% of that of all the flow parts, and the disk friction loss caused by the surface roughness of all the flow parts accounts for 74.26% of all the increasing shaft power, which indicates that the increasing shaft power caused by the surface roughness is mainly caused by the disk friction loss which is also mainly determined by the surface roughness of the outer wall of the shroud.

Figure 9 shows the mechanical efficiency $\eta_m$, the hydraulic efficiency $\eta_h$ and the volumetric efficiency $\eta_v$ for different roughness groups at rated flow condition. Combined with Table 6, it can be seen that the surface roughness of the impeller and the diffuser mainly affects $\eta_h$. Moreover, the surface roughness of the outer wall of the shroud mainly influences $\eta_m$, while that of the inner wall of the pump cavity mainly affects $\eta_v$. The comprehensive influence of the surface roughness of all the flow parts on the pump efficiency is smaller than the sum influence of that of each flow parts, indicating once again that the influence of the surface roughness on the pump performance is interconnected.

**TABLE 7.** Pump's performance with different flow rate and surface roughness.

| $Q$ (m$^3$/h) | $\mu$ (μm) | $H$ (m) | $P_m$ (W) | $P_h$ (W) | $q$ (m$^3$/h) | $\eta_m$ (%) | $\eta_v$ (%) | $\eta_h$ (%) | $\eta$ (%) |
|---|---|---|---|---|---|---|---|---|---|
| 1.65 | 0 | 56.00 | 53.72 | 585.70 | 0.87 | 74.36 | 65.61 | 65.46 | 31.94 |
| 2.64 | 0 | 47.88 | 44.46 | 668.67 | 0.74 | 77.81 | 78.06 | 65.92 | 40.04 |
| 3.30 | 0 | 41.83 | 37.83 | 717.66 | 0.68 | 79.58 | 82.98 | 63.10 | 41.67 |
| 3.96 | 0 | 35.28 | 30.43 | 754.08 | 0.63 | 81.02 | 86.32 | 58.43 | 40.86 |
| 5.40 | 0 | 15.13 | 7.81 | 756.22 | 0.47 | 82.97 | 91.92 | 32.00 | 24.41 |
| 1.65 | 40 | 53.72 | 53.72 | 623.15 | 1.04 | 66.21 | 61.38 | 63.08 | 25.64 |
| 2.64 | 40 | 44.46 | 44.46 | 704.60 | 0.90 | 70.00 | 74.55 | 60.83 | 31.74 |
| 3.30 | 40 | 37.83 | 37.83 | 755.01 | 0.83 | 72.12 | 79.948 | 56.30 | 32.46 |
| 3.96 | 40 | 30.43 | 30.43 | 798.08 | 0.76 | 73.93 | 83.98 | 48.94 | 30.38 |
| 5.40 | 40 | 7.81 | 7.81 | 787.51 | 0.51 | 75.14 | 91.39 | 15.60 | 10.96 |

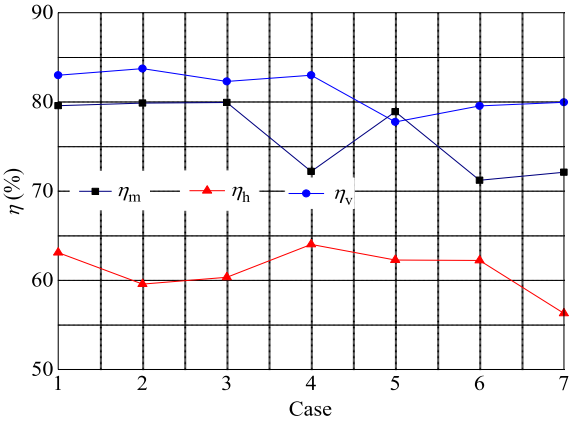


**FIGURE 9.** Pump's mechanical, hydraulic and volumetric efficiency with different roughness groups.

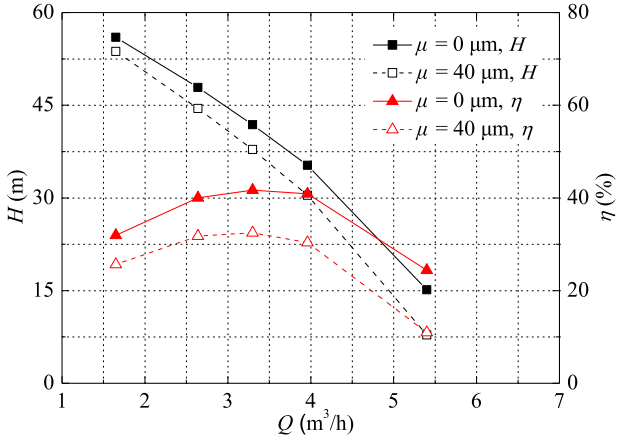


**FIGURE 10.** Pump's head and efficiency with two surface roughness at different flow conditions.

High power and low efficiency are the main problems easily appearing in the centrifugal pump. The above study shows that the surface roughness has a great effect on the efficiency and the power of the pump. Especially, reducing the surface roughness of the shroud and the pump cavity can significantly improve the pump efficiency and reduce the pump power. Therefore, due to that it's difficult to do the finish machining in the impeller and the diffuser, polishing the outer wall of the shroud and the inner wall of the pump cavity is an effective way to improve the pump performance.

### *D. THE INFLUENCE OF THE SURFACE ROUGHNESS ON THE PUMP PERFORMANCE AT DIFFERENT FLOW CONDITIONS*

According to different working occasions, the flow conditions of the pump will change. In order to further study the influence of the surface roughness on the pump performance at different flow conditions, five flow conditions and two surface roughnesses were selected in the following numerical calculations. The numerical results are shown in Table 7.

Figure 10 shows the head $H$ and the efficiency $\eta$ of the pump with two surface roughness at different flow conditions. Combined with Table 7, it can be seen that $H$ and $\eta$ decreases together after $\mu$ is taken into consideration. What's more, with the increase of $Q$, the negative effect of $\mu$ on $H$ and $\eta$ is enhanced. When $Q = 1.65$ m$^3$/h, the $\mu$ of 40 $\mu$m will lead to 2.28 m reduction of $H$ and 6.30 percentage points reduction of $\eta$. When $Q = 5.4$ m$^3$/h, the $\mu$ of 40 $\mu$m leads to 7.32 m reduction of $H$ and 13.47 percentage points reduction of $\eta$. The results indicate that the larger the flow rate, the greater the Reynolds number, and the improvement of the head and the efficiency is more apparent due to the reduction of the surface roughness.

Figure 11 shows the disk friction loss power $P_m$, the hydraulic power $P_h$ and the shaft power $P$ of the pump with two surface roughnesses at different flow conditions. Combined with Table 7, it is found that, with the increase of $Q$, $P_m$ keeps decreasing, while $P_h$ and $P$ first increase and then decrease. It indicates that $P$ has a maximum value,

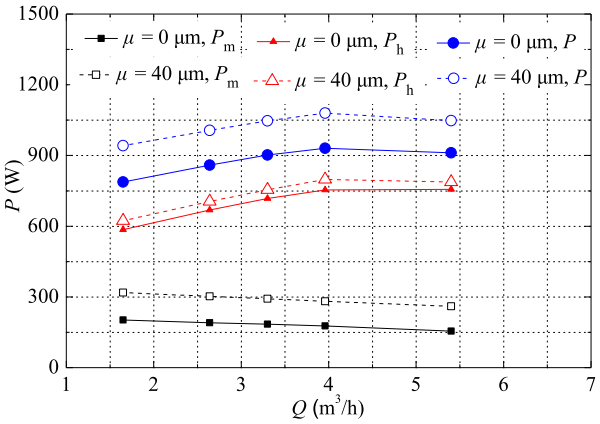


**FIGURE 11.** Pump's disk friction loss power, hydraulic power and shaft power with two surface roughness at different flow conditions.

which makes the non-overload characteristic of the pump. After considering the surface roughness, three kinds of power increase together, but the increasing rate remains unchanged with the increase of $Q$, which declares that the influence of the surface roughness on the shaft power is almost not affected by the Reynolds number.

Figure 12 shows the mechanical efficiency $\eta_m$, the hydraulic efficiency $\eta_h$ and the volumetric efficiency $\eta_v$ of the pump with two surface roughness at different flow conditions. Combined with Table 7, it can be seen that, with the increase of $Q$, $P_m$ and $q$ decrease constantly, leading to the increase of $\eta_m$ and $\eta_v$, but the increasing rate decreases gradually. Moreover, there is large volumetric leakage at the front ring of the pump under small flow condition, which leads to that the theoretical flow rate of the pump is close to the optimum flow rate of the impeller at this time. Therefore, $\eta_h$ becomes relatively large under small flow condition and then decreases gradually. After considering the surface roughness, $\eta_m$, $\eta_v$ and $\eta_h$ reduce together. With the increase of $Q$, the increment of $P_m$ caused by the surface roughness remains unchanged.

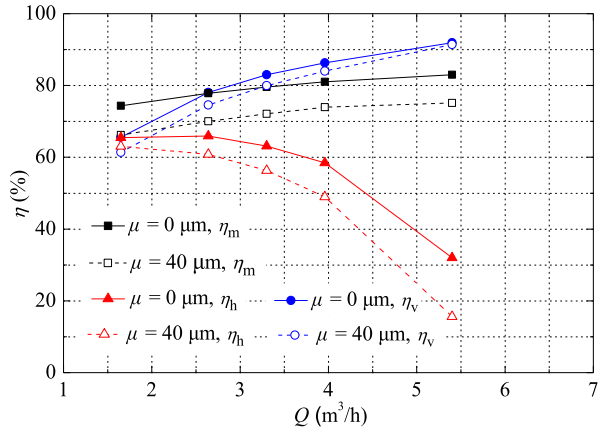


**FIGURE 12.** Pump's mechanical, hydraulic and volumetric efficiency at different flow conditions.

As a result, the decrement of $\eta_m$ caused by the surface roughness keeps also stable. With the increase of $Q$, $q/Q$ decreases constantly, so the variation of the volumetric leakage caused by the surface roughness decreases as well, leading to that the decrement of $\eta_v$ caused by the surface roughness decreases. With the increase of $Q$, the frictional head loss also increases, so the decrement of $\eta_h$ caused by the surface roughness increases instead.

### E. THE INFLUENCE OF THE SURFACE ROUGHNESS ON THE PUMP PERFORMANCE AT DIFFERENT ROTATIONAL SPEEDS

Through the above study, it can be found that, with the increase of the surface roughness, the hydraulic friction coefficient of the flow parts in the pump will also increase, leading to the sharp rise of the frictional head loss and the decrease of the hydraulic efficiency. Moreover, the mechanical efficiency is mainly decided by the disk friction loss power, on which there're lots of calculating formulas. Three typical formulas are shown as follow [38]–[40].

$$P_m = 0.133 \times 10^{-3} \rho R_d^{0.134} \omega^3 (D_2/2)^3 D_2^2 \quad (11)$$

$$P_m = 0.35 \times 10^{-2} \times k \rho \omega^3 (D_2/2)^5 \quad (12)$$

$$P_m = 1.1 \times 75 \times 10^{-6} \times \rho g u_2^3 D_2^2 \quad (13)$$

where $R_d = 10^6 \times \omega(D_2/2)^2$ and $\omega = 2\pi n/60$, $\omega$ is the angular velocity (in rad/s), $\rho$ is the density of the fluid (in kg/m$^3$), $k = 0.8$-$1$, $u_2$ is the circumferential speed of impeller outlet (in m/s).

It can be found in the empirical formulas that $P_m$ is directly proportional to $\rho$, $n^3$ and $D_2^5$, and that the effect of the surface roughness is totally ignored. In order to further study the effect of the roughness on the pump performance, three rotational speeds of $n = 700$, 1400, 2800 r/min were selected for the numerical calculations of the pump at rated flow condition with two surface roughness. The numerical results are demonstrated in Table 8. It can be seen that $P_m$ and $P_h$ of the pump with the rough disk are both larger than that with the smooth disk under three rotational speeds. With the increase of $n$, the increasing rate of $P_m$ keeps growing. When $n = 700$ r/min, the $\mu$ of 40 $\mu$m will make $P_m$ increase from 3.56 W to 4.70 W, which increases by 32.08%. When $n = 2800$ r/min, $P_m$ will increase by 58.52%, which indicates that the increase of the rotational speed will enhance the effect of the surface roughness on the disk friction loss power of the pump [41].

Figure 13 shows the mechanical efficiency $\eta_m$, the hydraulic efficiency $\eta_h$ and the volumetric efficiency $\eta_v$ of the pump with two surface roughness at different rotational speeds. When $\mu = 0$ $\mu$m, with the increase of $n$, $\eta_m$, $\eta_h$ and $\eta_v$ keep an increasing trend due to the increase of Re, while $\eta_m$, $\eta_h$ and $\eta_v$ keep a stable trend if $\mu = 40$ $\mu$m. Moreover, when $n = 700$ r/min, the $\mu$ of 40 $\mu$m will lead to 5.46 percentage points reduction of $\eta$, while $\eta$ will decrease by 9.21 percentage points if $n = 2800$ r/min, which indicating the surface roughness has a more significant inhabiting effect on the pump efficiency at high rotational speed.

**TABLE 8.** Pump's performance with different rotational speed with two surface roughness.

| $n$ (rpm) | $\mu$ (μm) | $P_m$ (W) | $P_h$ (W) | $Q$ (m$^3$/h) | $q$ (m$^3$/h) | $\eta_m$ (%) | $\eta_v$ (%) | $\eta_h$ (%) | $\eta$ (%) |
|---|---|---|---|---|---|---|---|---|---|
| 700 | 0 | 3.56 | 11.52 | 0.825 | 0.20 | 76.41 | 80.79 | 60.07 | 37.08 |
| 1400 | 0 | 25.75 | 90.89 | 1.65 | 0.36 | 77.92 | 81.92 | 61.53 | 39.27 |
| 2800 | 0 | 184.16 | 717.66 | 3.30 | 0.68 | 79.58 | 82.98 | 63.10 | 41.67 |
| 700 | 40 | 4.70 | 11.86 | 0.825 | 0.22 | 71.62 | 79.24 | 55.92 | 31.74 |
| 1400 | 40 | 36.94 | 94.61 | 1.65 | 0.42 | 71.92 | 79.72 | 55.90 | 32.05 |
| 2800 | 40 | 291.93 | 755.01 | 3.30 | 0.83 | 72.12 | 79.95 | 56.30 | 32.46 |

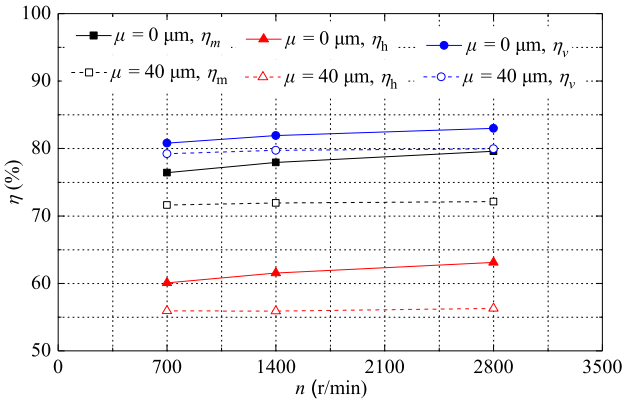


**FIGURE 13.** Pump's mechanical, hydraulic and volumetric efficiency at different rotational speeds.

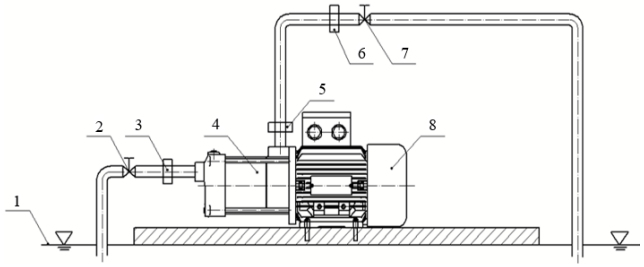


1. Pool 2. Inlet control valve 3. Inlet pressure transmitter 4. Pump 5. Outlet pressure transmitters 6. Turbine flowmeter 7. Flow control valve 8. Motor

**FIGURE 14.** Schematic diagram of the test rig.

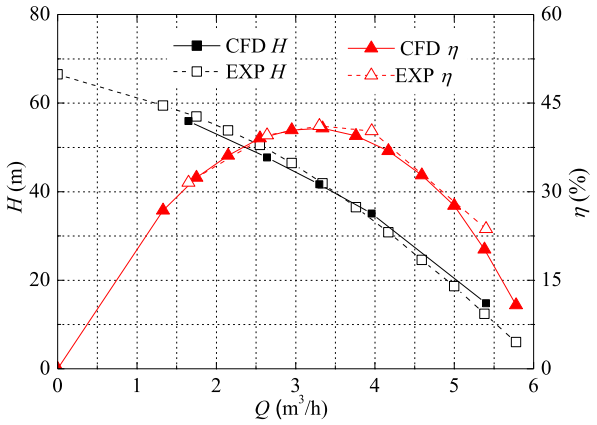


**FIGURE 15.** Numerical and experimental results of the pump's head and efficiency.

## IV. COMPARISON BETWEEN THE NUMERICAL AND EXPERIMENTAL RESULTS

Based on the above research, the whole field numerical calculations on the two-stage pump were made with the grid size of 0.8 mm, Standard $k$-$\varepsilon$ turbulence model, convergence precision of $10^{-5}$ and surface roughness of 1 $\mu$m. The simulations were performed at five flow points ($Q$ = 1.65, 2.94, 3.3, 3.96, 5.4 m$^3$/h). At the same time, the hydraulic models were sent to a pump company in Fujian Province and a five-stage centrifugal pump was manufactured. Then, the pump was sent to the Mechanical Products Testing Centre in Fujian Academy of Mechanical Sciences for the performance testing. As shown in Figure 14, the test rig is an open-type system, which is composed of two parts, namely, the acquisition system and the water circulation system. A turbine flowmeter was used to measure the flow rate $Q$ with the precision of ±0.3%. Speed of the pump $n$ is measured by a tachometer (PROVA RM-1500, Taiwan) with the precision of ±0.04%. During the experiment, two pressure transmitters (CYG1401) with the precision of ±0.2% were used to measure the inlet and outlet pressure.

The comparisons between the numerical and experimental results are displayed in Figure 15. In general, the predicted $H$ and $\eta$ are in good agreement with the experimental results at different flow conditions, particularly at rated flow condition ($Q$ = 3.3m$^3$/h) which are almost coincident. Under the non-rated flow conditions, due to the flow separation or recirculation in the pump, there is some discrepancy between the numerical and experimental results, but the deviation is still within 3%. The results show that, based on the whole calculation model and appropriate numerical setting method, it is creditable to predict the performances of multistage centrifugal pump using CFD.

## V. CONCLUSION

(1) The surface roughness is proved to have a significant influence on the pump performance. With the increase of the surface roughness, the head and the efficiency of the

pump decreases continuously, but the decreasing rate slows down gradually, and the surface roughness has a greater influence on the efficiency than on the head. Moreover, with the increase of the surface roughness, the disk friction loss power and the hydraulic power increase continuously, but the increasing rate decreases gradually, and the influence of the surface roughness on the disk friction loss power is much greater than that on the hydraulic power. In addition, with the increase of the surface roughness, the mechanical efficiency, the hydraulic efficiency and the volume efficiency decrease together, but the decreasing rate reduces constantly, and the total efficiency of the pump reduces mainly by decreasing the hydraulic efficiency and the mechanical efficiency, due to the negative effect of the surface roughness.

(2) The influence order of the surface roughness on the head is impeller, diffuser, shroud and pump cavity in sequence, while that on the efficiency is successively impeller, diffuser, pump cavity and shroud. The surface roughness of the impeller and the diffuser mainly affects the hydraulic efficiency. Moreover, the surface roughness of the outer wall of the shroud mainly influences the mechanical efficiency, while that of the inner wall of the pump cavity mainly affects the volume efficiency. The comprehensive influence of the surface roughness of all the flow parts on the pump efficiency is smaller than the sum influence of that of each flow parts, indicating that the influence of the surface roughness on the pump performance is interconnected.

(3) With the increase of the flow rate, the negative effect of the surface roughness on the head and the efficiency is enhanced, while that on the shaft power keeps stable. What's more, the disk friction loss power of the pump with the rough disk are larger than that with the smooth disk, and the increasing rate of the disk friction loss power keeps growing with the increase of the rotational speed. Additionally, the surface roughness has a more significant inhabiting effect on the pump efficiency and promoting effect on the disk friction loss power at high rotational speed.

(4) Numerical and experimental results are almost coincident under rated flow condition, but there are some minor discrepancies (within 3%) under non-rated flow conditions because of flow separation or recirculation in the pump. Therefore, it is rather creditable to predict the performances of multistage centrifugal pump using CFD based on the whole calculation model and appropriate numerical setting methods.

(5) For general multistage centrifugal pumps, reducing the volumetric leakage loss and interstage leakage loss is the most effective way to increase the efficiency of centrifugal pump. In addition, due to the fact that it is very difficult to make the precision-machine inside the impeller and diffuser, polishing the impeller shroud and pump cavity is beneficial to improve the pump efficiency and reduce the pump shaft power.

## REFERENCES

[1] Q. Li, M. Liu, J. Zhang, and Q. Liu, "Flow characteristic of guide vane region in turbine braking operation of pump-turbine," *J. Drainage Irrigation Mach. Eng.*, vol. 35, no. 6, pp. 495–501, Jun. 2017.
[2] Y. Lu, R. Zhu, X. Wang, C. An, Y. Zhao, and Q. Fu, "Experimental study on transient performance in the coasting transition process of shutdown for reactor coolant pump," *Nucl. Eng. Des.*, vol. 346, pp. 192–199, May 2019.
[3] H. Chang, W. Shi, W. Li, and J. Liu, "Energy loss analysis of novel self-priming pump based on the entropy production theory," *J. Therm. Sci.*, vol. 28, no. 2, pp. 306–318, 2019.
[4] C. Wang, W. Shi, X. Wang, X. Jiang, Y. Yang, W. Li, and L. Zhou, "Optimal design of multistage centrifugal pump based on the combined energy loss model and computational fluid dynamics," *Appl. Energy*, vol. 187, pp. 10–26, Feb. 2017.
[5] C. Wang, X. He, D. Zhang, B. Hu, and W. Shi, "Numerical and experimental study of the self-priming process of a multistage self-priming centrifugal pump," *Int. J. Energy Res.*, vol. 43, no. 9, pp. 4074–4092, Jul. 2019.
[6] H. Chang, W. Li, W. Shi, and J. Liu, "Effect of blade profile with different thickness distribution on the pressure characteristics of novel self-priming pump," *J. Brazilian Soc. Mech. Sci. Eng.*, vol. 40, no. 11, p. 518, 2018.
[7] Q. Li, W. Li, L. Ji, W. Shi, X. Zhao, and X. Jiang, "The experimental research on axis orbit of mixed-flow pump," *Trans. Can. Soc. Mech. Eng.*, vol. 41, no. 5, pp. 745–757, Dec. 2017.
[8] X. Li, Z. Jiang, Z. Zhu, Q. Si, and Y. Li, "Entropy generation analysis for the cavitating head-drop characteristic of a centrifugal pump," *Proc. Inst. Mech. Eng. C, J. Mech. Eng. Sci.*, vol. 232, no. 24, pp. 4637–4646, Jan. 2018.
[9] R. Gao, L. Yuan, M. Yu, and W. Liu, "Effects of heat pump drying parameters on the volatile flavor compounds in silver carp," *J. Aquatic Food Product Technol.*, vol. 25, no. 5, pp. 735–744, Jan. 2016.
[10] C. Xia, L. Cheng, C. Luo, W. Jiao, and D. Zhang, "Hydraulic characteristics and measurement of rotating stall suppression in a waterjet propulsion system," *Trans. FAMENA*, vol. 42, no. 4, pp. 85–100, Dec. 2018.
[11] H. Wang, H. Li, and C. Zou, "Experiment study on device performance of swirling jet pump," *J. Drain. Irrigation Mach. Eng.*, vol. 35, no. 4, pp. 283–288, Apr. 2017.
[12] J. Feng, H. Liu, J. Ding, X. Wu, and L. Dong, "Status of study on single channel centrifugal pumps and its developing tendency," *J. Drainage Irrigation Mach. Eng.*, vol. 35, no. 3, pp. 207–215, Mar. 2017.
[13] G. Lin, J. Yuan, Q. Si, B. Zhou, and W. Sun, "Effect of impeller geometric parameters on characteristics of inlet recirculation in centrifugal pump," *J. Drainage Irrigation Mach. Eng.*, vol. 35, no. 2, pp. 106–112, Feb. 2017.
[14] X. Fangwei, X. Ri, S. Gang, and W. Cuntang, "Flow characteristics of accelerating pump in hydraulic-type wind power generation system under different wind speeds," *Int. J. Adv. Manuf. Technol.*, vol. 92, nos. 1–4, pp. 189–196, Feb. 2017.
[15] H. Chen, T. Zhang, and C. Wang, "Structural characteristics of ultrahigh-pressure multistage centrifugal pump typed SDZ310," *J. Drainage Irrigation Mach. Eng.*, vol. 36, no. 7, pp. 567–572, Jul. 2018.
[16] C. Wang, X. Chen, N. Qiu, Y. Zhu, and W. Shi, "Numerical and experimental study on the pressure fluctuation, vibration, and noise of multistage pump with radial diffuser," *J. Brazilian Soc. Mech. Sci. Eng.*, vol. 40, no. 10, p. 481, Oct. 2018.
[17] Z. Lu, C. Wang, N. Qiu, W. Shi, X. Jiang, Q. Feng, and W. Cao, "Experimental study on the unsteady performance of the multistage centrifugal pump," *J. Brazilian Soc. Mech. Sci. Eng.*, vol. 40, no. 5, p. 264, May 2018.
[18] Z. Lu, Q. Liu, K. Wang, and K. Cheng, "Worldwide technical analysis on multistage centrifugal pump based on patent map," *J. Drainage Irrigation Mach. Eng.*, vol. 35, no. 3, pp. 216–221, Mar. 2017.
[19] C. Wang, X. He, W. Shi, X. Wang, X. Wang, and N. Qiu, "Numerical study on pressure fluctuation of a multistage centrifugal pump based on whole flow field," *AIP Adv.*, vol. 9, no. 3, Mar. 2019, Art. no. 035118.
[20] R. Xie, F. Tang, S. Li, L. Shi, and F. Yang, "Cross-section unbalanced force among impellers of five-stage centrifugal pump," *J. Drainage Irrigation Mach. Eng.*, vol. 35, no. 10, pp. 842–848, Oct. 2017.
[21] W. Zhou, N. Qiu, L. Wang, B. Gao, and D. Liu, "Dynamic analysis of a planar multi-stage centrifugal pump rotor system based on a novel coupled model," *J. Sound Vib.*, vol. 434, pp. 237–260, Nov. 2018.
[22] Z. Lu, X. He, and C. Wang, "Influencing factors of self-priming time of multistage self-priming centrifugal pump," *DYNA*, vol. 93, no. 6, pp. 1–13, Nov. 2018.
[23] C. Wang, B. Hu, Y. Zhu, X. Wang, C. Luo, and L. Cheng, "Numerical study on the gas-water two-phase flow in the self-priming process of self-priming centrifugal pump," *Processes*, vol. 7, no. 6, p. 330, Jun. 2019.
[24] C. Wang, W. Shi, Q. Si, and L. Zhou, "Numerical calculation and finite element calculation on impeller of stainless steel multistage centrifugal pump," *J. Vibroeng.*, vol. 16, no. 4, pp. 1723–1734, Jun. 2014.

[25] A. J. Stepanoff, *Centrifugal and Axial Flow Pumps: Theory, Design, and Application*. Beijing, China: Machine Press, 1980.
[26] A. Lomakin, *Centrifugal and Axial Pump*. Beijing, China: Machine Press, 1978.
[27] L. Li and Z. Wang, "Simulation of the influence of wall roughness on the performance of axial-flow pumps," *Trans. Chin. Soc. Agricult. Eng.*, vol. 20, no. 1, pp. 132–135, Jan. 2014.
[28] Y. Wei, H. Yang, H.-S. Dou, Z. Lin, Z. Wang, and Y. Qian, "A novel two-dimensional coupled lattice Boltzmann model for thermal incompressible flows," *Appl. Math. Comput.*, vol. 339, no. 15, pp. 556–567, Dec. 2018.
[29] S. Zhang, X. Li, B. Hu, Y. Liu, and Z. Zhu, "Numerical investigation of attached cavitating flow in thermo-sensitive fluid with special emphasis on thermal effect and shedding dynamics," *Int. J. Hydrogen Energy*, vol. 44, no. 5, pp. 3170–3184, Jan. 2019.
[30] X. Li, B. Li, B. Yu, Y. Ren, and B. Chen, "Calculation of cavitation evolution and associated turbulent kinetic energy transport around a NACA66 hydrofoil," *J. Mech. Sci. Technol.*, vol. 33, no. 3, pp. 1231–1241, Mar. 2019.
[31] Y. Lu, R. Zhu, Q. Fu, X. Wang, C. An, and J. Chen, "Research on the structure design of the LBE reactor coolant pump in the lead base heap," *Nucl. Eng. Technol.*, vol. 51, no. 2, pp. 546–555, Oct. 2018.
[32] L. Yonggang, Z. Rongsheng, W. Xiuli, W. Yang, F. Qiang, and Y. Daoxing, "Study on the complete rotational characteristic of coolant pump in the gas-liquid two-phase operating condition," *Ann. Nucl. Energy*, vol. 123, pp. 180–189, Jan. 2019.
[33] X. Wang, B. Zhu, S. Cao, and L. Tan, "Optimal design of reversible pump-turbine runner," *Trans. Chin. Soc. Agricult. Eng.*, vol. 30, no. 13, pp. 78–85, Jul. 2014.
[34] J. S. Anagnostopoulos, "A fast numerical method for flow analysis and blade design in centrifugal pump impellers," *Comput. Fluids*, vol. 38, no. 2, pp. 284–289, Feb. 2009.
[35] J.-H. Kim, H.-C. Lee, J.-H. Kim, S. Kim, J.-Y. Yoon, and Y.-S. Choi, "Design techniques to improve the performance of a centrifugal pump using CFD," *J. Mech. Sci. Technol.*, vol. 29, no. 1, pp. 215–225, Jan. 2015.
[36] S. Derakhshan, M. Pourmahdavi, E. Abdolahnejad, A. Reihani, and A. Ojaghi, "Numerical shape optimization of a centrifugal pump impeller using artificial bee colony algorithm," *Comput. Fluids*, vol. 81, pp. 145–151, Jul. 2013.
[37] W. Shi, H. Li, W. Lu, J. Dai, and X. Li, "Effect of prewhirl flow on non-overload performance of low-specific-speed centrifugal pumps," *Trans. CSAE*, vol. 44, no. 5, pp. 50–54, May 2013.
[38] D. Luo and S. Liu, "Experimental study on the disk friction loss of low-specific-speed centrifugal pumps," *J. Drainage Irrigation Mach. Eng.*, vol. 7, no. 3, pp. 4–7, Mar. 1989.
[39] S. Li and S. Liu, "Experimental study on the disk friction loss of low-specific-speed centrifugal pumps," *Pump Technol.*, vol. 33, no. 3, pp. 21–25, 1988.
[40] H. Liu, M. Tan, and S. Yuan, "Calculation of disk friction loss of centrifugal pumps," *Trans. Chin. Soc. Agricult. Eng.*, vol. 22, no. 12, pp. 107–109, Dec. 2006.
[41] W. Li, Z. Xu, and F. Lu, "Experimental study of the disk friction loss in the pumps," *Trans. Chin. Soc. Agricult. Eng.*, vol. 29, no. 2, pp. 58–61, Jun. 1998.

**XIAOKE HE** is currently a Lecturer with the School of Electric Power, North China University of Water Resources and Electric Power. His research interests include modern pump design theory and method, numerical analysis of the internal flow field in a centrifugal pump, and renewable energy utilization technology. In the past few years, he has published more than 10 high-quality academic papers.

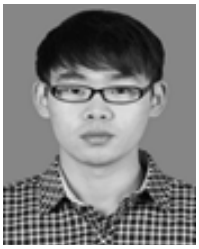

**WEIXUAN JIAO** is currently pursuing the Ph.D. degree with Yangzhou University, China. His research interest includes numerical simulation of the pump.

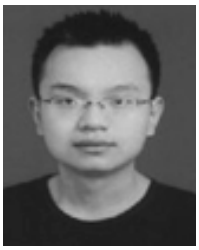

**CHUAN WANG** is currently an Associated Professor with Yangzhou University and the North China University of Water Resources and Electric Power. His research interests include optimal design of centrifugal pump and internal flow of jet. In the past several years, he has published more than 20 high-quality academic papers.

**WEIDONG CAO** is currently an Associate Professor with the Institute of Fluid Engineering Equipment, Jiangsu University. His research interest includes the optimal design of the pump. In the past several years, he has published more than 10 high-quality academic papers.